

Shear induced migration during suspension transport in regular and random porous media

*Rupak Bhowmik**, *Vikas Kumar Sharma*, and *Anugrah Singh*

Department of Chemical Engineering, Indian Institute of Technology Guwahati, Assam-781039, India

Suspension transport in porous media is crucial in various industrial and natural processes, influenced by the intricate structure and interactions within the porous framework. This study investigates suspension transport in regular and random porous media using numerical simulations based on a continuum Diffusive Flux Model. The flow visualization experiments with Micro Particle Image Velocimetry were also conducted in porous micromodels. We have analysed the velocity and particle concentration fields to gain insights into the transport dynamics. In regular arrangements, specific configurations caused wavy flow paths that enhanced particle migration. The random porous media forced particles through multiple tortuous pathways, clustering near pore throats instead of migrating toward the centre, typical of channel flows. Our numerical results closely matched the experimental data. The experiments also assessed single-particle dynamics and concentrated suspension flows, demonstrating that initial particle positions significantly affect trajectory outcomes, consistent with prior Stokesian dynamics simulations. Particles near the grains experienced prolonged retention due to complex paths and strong hydrodynamic interactions. Higher particle concentrations resulted in cluster formation, leading to velocity drift, while dilute suspensions showed significant fluctuations, highlighting the concentration-dependent transport behaviour in porous media.

1 Introduction

Particle migration in porous media is a critical phenomenon influencing both natural processes and engineered applications. A thorough understanding of suspension flow dynamics is essential for understanding these processes. Shear Induced Particle Migration (SIPM) has been extensively investigated through experiments, simulations, and numerical analyses in various flow configurations. Recent research in shear-induced particle migration has extensively utilized both the Diffusive Flux Model (DFM) originally developed by Phillips et al. [1] and the Suspension Balance Model (SBM) originally formulated by Nott and Brady [2] and later modified by Morris and Boulay [3]. The DFM describes particle migration through diffusive fluxes driven by concentration and viscosity gradients, while the SBM explains migration through particle stress gradients rather than diffusive processes. Howard et al. [4] developed comprehensive bidisperse SBM frameworks demonstrating that particle stresses distribute proportionally to relative volume fractions, with large particles forming streamwise chains in wall layers. Kang and Mirbod [5] conducted numerical simulations using the DFM, showing that migration magnitude is often lower than SBM predictions, particularly for semi-dilute suspensions. Reddy and Singh [6] investigated bidisperse suspension flows using the DFM, demonstrating that larger particles consistently enrich the channel centre. Orsi et al. [7]

provided detailed validation of SBM using particle-resolved simulations, showing fair agreement except in areas near the boundaries and channel centres. Particle migration in porous media is governed by hydrodynamic forces, geometric straining, and particle-wall interactions. Liu et al. [8] used microfluidic chips to reveal clogging and retention mechanisms under convergent radial flow, highlighting electrostatic and inertial effects at pore throats. De and Singh [9] employed Stokesian dynamics simulations in heterogeneous dual-porosity media, demonstrating enhanced migration across concentration and porosity gradients. However, limited literature addresses the application of DFM or SBM in the studies specific to the porous media flow. The original DFM was only applicable to simple planar and unidirectional flows. Krishnan et al [16] proposed effect of curvature induced flux in geometries with curved streamlines. However, DFM model incorporated several phenomenological constants. The SBM provides a more unified approach to particle migration by considering the anisotropic stresses. Recent studies have developed frame-invariant SBM formulations. Miller et al.[11], Dbouk [12] [14] and Dbouk et al. [13] demonstrated the effectiveness of frame invariant SBM in capturing particle migration and normal stresses in complex flow domains, highlighting its effectiveness in realistic suspension transport modelling.

Due to strong coupling between the flow and rheology the SBM requires more computational power

* Corresponding author: rprupak@iitg.ac.in

compared to the DFM. The DFM requires solving simpler governing equations avoiding the computationally intensive particle stress tensor calculations demanded by SBM [10]. We have chosen DFM in the present studies mainly due to its low computational cost and better numerical stability while performing pore scale simulations with large number of grain particles. Experimental validation demonstrates that DFM implementations achieve acceptable accuracy while maintaining significantly lower computational costs [10]. The modified frame-invariant DFM further enhances these advantages by incorporating curvature effects crucial for complex porous geometries [15,16]. We have also considered curvature induced flux since the flow path in a porous system is highly tortuous.

2 Numerical Method

The suspension is considered a continuous medium in the continuum model, and the behavior of the suspension is governed by the conservation of mass, momentum, and particle equations. The DFM proposed by Philips et al. [1] and modified by Krishnan et al. [16] was used in this work. The continuity and momentum equations for incompressible, monodispersed, neutrally buoyant, and non-Brownian suspension flow are given as:

$$\nabla \cdot \vec{v} = 0, \quad (1)$$

$$\rho(\vec{v} \cdot \nabla) \vec{v} = -\nabla p + \nabla \cdot [\eta(\nabla \vec{v} + \nabla \vec{v}^T)], \quad (2)$$

$$\frac{\partial}{\partial t}(\phi) + \vec{v} \cdot \nabla \phi = -\nabla \cdot \vec{N}_t, \quad (3)$$

where, \vec{v} is the velocity, p is the pressure, $\rho = 1190 \text{ kg/m}^3$ is the density, and η is the viscosity of the suspension, which depends on the volume fraction of particles (ϕ) in the suspension given by Krieger[17] as follows:

$$\eta(\phi) = \eta_0 \left(1 - \frac{\phi}{\phi_m}\right)^{-1.82}, \quad (4)$$

where $\eta_0 = 0.48 \text{ cP}$ is the viscosity of the suspending fluid and $\phi_m = 0.68$ is the maximum flowable packing fraction for the hard sphere. The total migration flux \vec{N}_t accounts for different migration flux: migration induced by the gradient of shear rate (\vec{N}_c), viscosity (\vec{N}_η), and streamline curvature (\vec{N}_r). To address concentration discontinuities near the channel center in pressure-driven flows, a non-local shear rate term, following Miller and Morris [18], was implemented. Kindly see Reddy et al., Philips et al., and Krishnan et al. [16,1,6] for further details. The governing equations were solved simultaneously using OpenFOAM v9, discretized via the finite volume method with a Gauss linear spatial scheme and a Euler temporal scheme. Pressure-velocity coupling was handled by the PISO algorithm. The pressure is solved using the Preconditioned Conjugate Gradient (PCG) solver with the Diagonal Incomplete Cholesky (DIC) preconditioner, while the particle volume fraction and velocity are solved using the Preconditioned Bi-Conjugate Gradient (PBiCG) with Diagonal-based Incomplete LU preconditioner (DILU) preconditioner. The bulk and particle Reynolds numbers are in the order of $O(10^{-2})$ and $O(10^{-3})$ for the simulation and experiments.

3 Experimental Method

A homogeneous porous micromodel was prepared using soft-lithography. The porosity of the micromodel was 0.78, with a cylinder (solid grains) diameter and pore throat of 800 and 500 μm , respectively. PMMA particles with a size of 40 μm and a density of 1.18 g/cm^3 were used and suspended in a glycerol-water solution with a ratio of 76:24 to make neutrally buoyant suspension. Suspensions with varying concentrations were injected into the porous media, and the flow dynamics were visualized using a μ -PIV setup. The details on soft lithography techniques for preparing the porous micro model, μ -PIV techniques, and post-processing of images can be found in Sharma et al. [19].

4 Results and Discussion

4.1 Single-particle flow dynamics

To examine single-particle dynamics suspension with low particle concentration (2.5 wt.%) was injected into the medium, and the trajectories of individual particles were meticulously tracked. The results demonstrate that particles released from the centre of the flow channel follow a less tortuous trajectory, resulting in reduced retention time as they traverse the medium. In contrast, particles released adjacent to fixed cylinders exhibit increased path tortuosity and retention time, with significant flow path deviation between channels. These observations closely align with the Stokesian dynamics simulations conducted by De and Singh [9], which delineates particle trajectories based on their release locations. Figure 1(a) presents the particle trajectories from experiments, while Figure 1(b) depicts particle trajectories from numerical simulations during suspension flow through the porous medium. A comparison between experimental velocity magnitudes for dilute suspension flow reveals a qualitative symmetry in velocity magnitude; despite the omission of particle-particle interactions in the simulations,

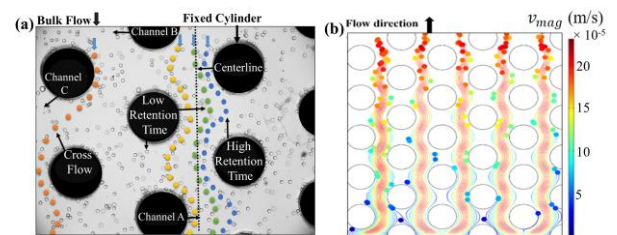


Figure 1: Particle trajectories during low-concentration suspension flow through the porous medium: (a) Experimental results, (b) Numerical simulation.

4.2 Experimental Analysis of Suspension Flow

Experiments were conducted to investigate suspension flow through a porous medium by injecting suspensions with particle concentrations of 2.5%, 5%, 7.5%, and 20%. At a concentration of 2.5%, the suspension exhibited a uniform, cluster-free flow (Figure 2(a)). Increasing the concentration to 5% led to the deposition of some particles at the base of cylinders and the

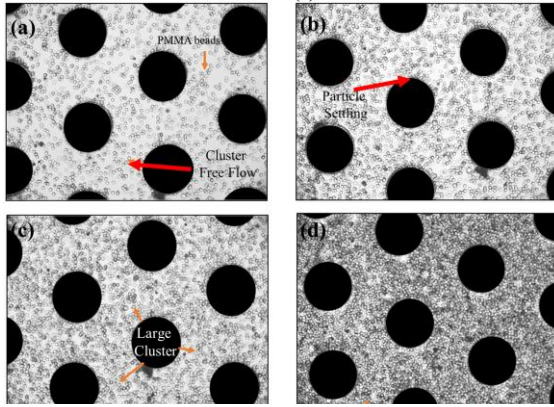


Figure 2: Suspension flow through the porous medium, (a) 2.5 wt.%, (b) 5 wt.%, (c) 7.5 wt.%, and (d) 20 wt. % PMMA.

formation of sparse clusters (Figure 2(b)). A further increase to 7.5% resulted in pronounced particle clustering (Figure 2(c)), while at 20%, severe clustering was observed (Figure 2(d)). Figure 3 demonstrates the velocity and concentration contour for a suspension of 20 wt.% PMMA flowing a flow rate of 0.05 ml/min.

At 2.5%, a maximum velocity of 0.97 mm/s was recorded, attributed to the absence of inter-particle interactions, and at 5%, interactions induced a negative drift velocity, reducing the maximum velocity to 0.78 mm/s. At 7.5%, this negative drift intensified, further decreasing the velocity to 0.53 mm/s. However, at 20%, the densely clustered particles, constrained by spatial limitations, moved cohesively in the flow direction, imparting additional momentum and elevating the velocity to 0.572 mm/s.

Concentration contour plots were generated using MATLAB for suspensions ranging from 2.5 to 20 wt.% (Figure 3(b)) elucidating the effect of particle concentration on flow behaviour within a homogeneous porous medium. It was observed that minimal particle concentrations were near microcylinders and maximal concentrations at pore throats, with the highest concentrations observed in the centre of the channel. The effect of particle concentration on the suspension flow characteristics can be clearly observed in Figure 2.

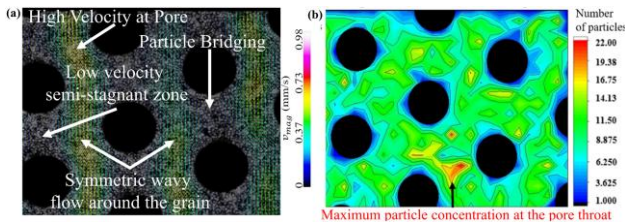


Figure 3: (a) The instantaneous velocity field and (b) Concentration contour w.r.t number of particles for suspension infiltrating at 0.05 ml/min in the 2D porous micromodel for suspension of 20 wt.% PMMA

4.3 Numerical Analysis of Suspension Flow

The simulations were performed in a two-dimensional porous medium, with cylinders aligned parallel to the flow direction. The inlet had uniform particle concentration and velocity, while the outlet was maintained at atmospheric pressure. No-slip and no-flux

boundary conditions were applied to all the walls and grain surfaces. The simulation domain was determined using 2D porous media with varying vertical pore spaces. The inlet particle volume fraction was 0.3 and the inlet velocity was 0.005 m/s. Simulations with pure fluid had established fully developed flow beyond the 7th pore space. The mesh convergence tests were also conducted to determine the optimum mesh resolutions. The REV of solid grain diameter 0.9 mm and throat size 0.3 mm was considered for the present study.

Figure 4(a,b) shows that velocity has its maximum at the pore-throat due to the sudden reduction in the flow area. As we move down from the pore throat to the pore space, the profile is considerably blunted compared to pure fluid. However, the change in the velocity is marginal at the center of the pore space. At the middle of the pore-throat (L1), the shear rate is higher at the wall, and thus, the particle migrated away from the wall, and the maximum particle volume fraction was observed at the centre of the channel (Figure 4(c,d,e)). As the particles move from the constricted pore throat to the pore space (L2, L3), the velocity decreases, and the shear-rate profile shows the peak-valley-peak pattern across the pore space. The centerline velocity of the pore-space region is lower than that of the pore-throat. The vertical pore-throat corresponds to a zero velocity and shear rate; consequently, a cloud of high-concentration particles was observed in these regions. The shear rate gradient leads the particles to migrate from the high-shear region to the low-shear region. Whereas, particles migrate from regions of high curvature to low curvature due to curvature-induced forces. On the other hand, the viscosity gradient leads to particles moving from high-concentration to low-concentration areas. The impact of curvature-induced flux can be clearly seen. In the presence of curvature-induced flux, particles migrate from the centre towards the wall of the vertical pore throat, whereas in its absence, migration occurs towards the centre.

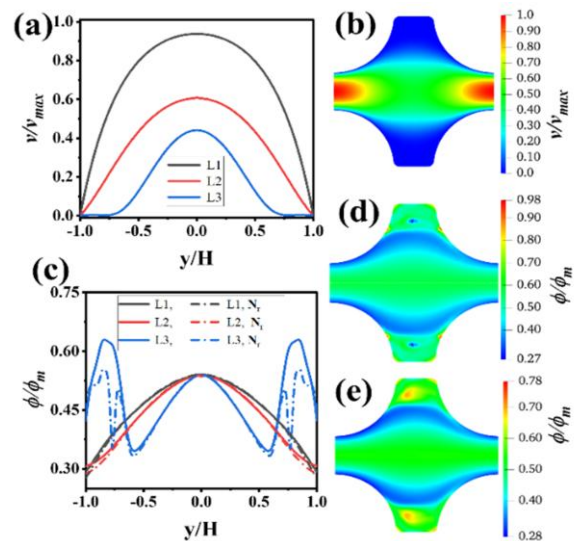


Figure 4: Numerical simulation: (a) velocity profile, (b) velocity contour, (c) volume fraction profile (Solid line represents without curvature and dash-dot line represents with curvature induced flux), and volume fraction contour for (d) with N_r , (e) without N_r

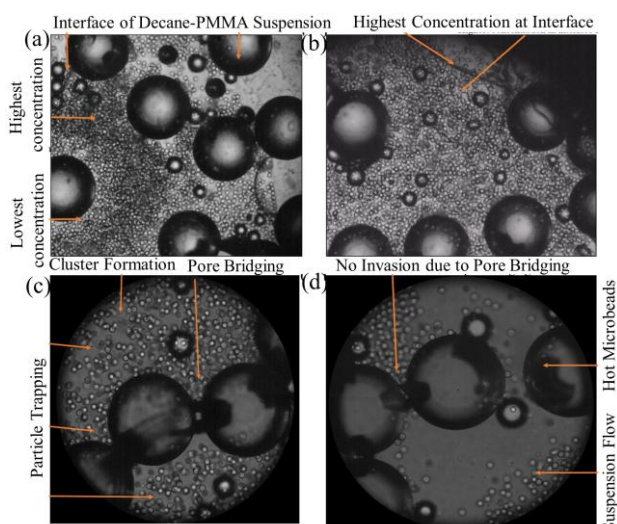


Figure 5: Multiphase displacement of suspension by n-decane: (a) shear-induced migration, (b) maximum concentration at the interface, (c)-(d) cluster formation, and pore bridging prevent the suspension flow through the pore throat.

4.4 Multiphase flow in heterogeneous media

A multiphase flow investigation was conducted in a heterogeneous porous medium saturated with a dense suspension comprising 5 wt.% PMMA particles. Subsequently, n-decane was injected at a constant flow rate of 0.05 ml/min to displace the suspension. During this process, particle accumulation was observed at the interface between the suspension and n-decane, where the particle concentration was highest, as shown in Figure 5. As the interface advanced, shear-induced particle migration caused a concentration gradient, with the maximum particle concentration occurring in the centre of the flow channel and low concentrations near the bead walls. The flow exhibited unsteady behaviour, leading to fluctuations in the displacement process. Interface tracking and velocity magnitude maps were generated over time to examine the dynamics further. Initially, the interface remained stationary, but upon injection of n-decane, a peak in velocity was observed at the interface, particularly in the central region of the channel, due to migration. Velocity decreased progressively ahead of the interface and within open pore spaces. Notably, higher velocities were detected in narrow pore constrictions. The porous medium's heterogeneity, governed by the pore throat-to-particle diameter ratio, resulted in particle trapping, bridging, and clustering; impeding flow through small pores as shown in Figure 5(c-d).

5 Conclusion

This study examines suspension flow through porous media using experiments and simulations. At low concentrations, the tortuosity affects the retention times. With increasing concentration, clustering alters velocity and induces shear-driven migration. The curvature-induced flux significantly influences particle migration in the pores. In homogeneous porous media, transport

remains symmetric and predictable; in heterogeneous media, complex pore architectures induce trapping, flow deviation, and concentration-dependent behaviour. While the current study investigates suspension transport using DFM, further studies can be extended to use SBM in further understanding suspension transport in porous media.

Acknowledgment

The authors would like to acknowledge the financial support received from SERB (project no CRG/2021/005121) and the computing facility of IIT Guwahati for computational resources.

References

- [1] R.J. Phillips, R.C. Armstrong, R.A. Brown, A.L. Graham, J.R. Abbott, *Phys. Fluids*. **4** 30–40 (1992).
- [2] P.R. Nott, J.F. Brady, *J. Fluid Mech.* **275** 157–199 (1994).
- [3] J.F. Morris, F. Boulay, *J. Rheol.* **43** 1213–1237 (1999).
- [4] A.A. Howard, M.R. Maxey, S. Gallier, *Phys. Rev. Fluids*. **7** 124301 (2022).
- [5] C. Kang, P. Mirbod, *Int. J. Multiph. Flow*. **126** 103239 (2020).
- [6] M.M. Reddy, A. Singh, *Phys. Fluids*. **31** (2019).
- [7] M. Orsi, L. Lobry, E. Lemaire, F. Peters, *J. Fluid Mech.* **998** A16 (2024).
- [8] Q. Liu, B. Zhao, J.C. Santamarina, *J. Geophys. Res.* **124** (2019).
- [9] N. De, A. Singh, **131** 473–502 (2020).
- [10] L. Schlatter, G.G. da Silva Ferreira, P.L. da Cunha Lage, *Int. J. Multiph. Flow*. **184** (2025).
- [11] R.M. Miller, J.P. Singh, J.F. Morris, *Chem. Eng. Sci.* **64** 4597–4610 (2009).
- [12] T. Dbouk, J. Nonnewton. *Fluid Mech.* **230** 68–79 (2016).
- [13] T. Dbouk, L. Lobry, E. Lemaire, *J. Fluid Mech.* **715** 239–272 (2013).
- [14] T. Dbouk, *Part. Sci. Technol.* **38** 782–791 (2020).
- [15] J.M. Kim, S.G. Lee, C. Kim, *J. Non Newton. Fluid Mech.* **150** 162–176 (2008).
- [16] G.P. Krishnan, S. Beimfohr, D.T. Leighton, *J. Fluid Mech.* **321** 371–393 (1996).
- [17] I.M. Krieger, *Adv. Colloid Interface Sci.* **3** 111–136 (1972).
- [18] R.M. Miller, J.F. Morris, *J. NonNewton. Fluid Mech.* **135** 149–165 (2006).
- [19] V.K. Sharma, R. Bhowmik, P. Tiwari, A. Singh, *J. Pet. Sci. Eng.* **212** (2022).